ResearchGate

See discussions, stats, and author profiles for this publication at: https://www.researchgate.net/publication/232290104

Transient Stability Enhancement of the Power System Interconnected with Wind Farm Using Generalized Unified Power Flow Controller with Simplex Optimized Self-tuning Fuzzy Damping S...

Article *in* International Review of Electrical Engineering · August 2012

CITATIONS
2

READS
170

2 authors:

Mete Vural
Gaziantep University
60 PUBLICATIONS **191** CITATIONS
SEE PROFILE

Kamil Çağatay Bayindir
Ankara Yildirim Beyazit University
76 PUBLICATIONS **581** CITATIONS
SEE PROFILE

Some of the authors of this publication are also working on these related projects:

Modeling of shunt active power filter View project

New Techno-Economic Indices For DC-DC Converters Operate Under Variable Loads Conditions. View project

All content following this page was uploaded by Mete Vural on 01 April 2014.

The user has requested enhancement of the downloaded file.

Praise Worthy Prize

International Review of Electrical Engineering (I.R.E.E.), Vol. 7, N. 4
ISSN 1827- 6660 *July - August 2012*

Transient Stability Enhancement of the Power System Interconnected with Wind Farm Using Generalized Unified Power Flow Controller with Simplex Optimized Self-Tuning Fuzzy Damping Scheme

A. M. Vural, K. C. Bayindir

Abstract – *Due to increasing penetration of wind power into traditional grid, co-working of synchronous generators with wind turbines is gaining attention in terms of system stability. This paper deals with the transient stability enhancement of such systems by generalized unified power flow controller (GUPFC) having grid frequency switching quasi multi-pulse converters. Besides independent real and reactive power flow control capability of the two series converters, one series converter is commissioned to damp synchronous/induction generator speed fluctuations by a self-tuning fuzzy damping scheme in which output scaling factor is adjusted on-line according to a second fuzzy rule-base defined on error and error-integral of the synchronous generator speed. Damping function is further enhanced via simplex optimized gains cascaded to fuzzy inference system. AC bus voltage and DC link voltage of GUPFC are effectively controlled by the shunt converter without disturbing other control loops.*

The comparative simulation studies are carried out on a hybrid simulation platform in which power network and converters with their control blocks are modeled in PSCAD, while only the fuzzy arrangement of the control blocks is executed in MATLAB by interfacing these two programs on-line. Different disturbance scenarios have shown that the proposed approach exhibits superior damping performance than standard fuzzy logic control or PI regulator. ***Copyright © 2012 Praise Worthy Prize S.r.l. - All rights reserved.***

Keywords: *Wind Power, Self-Excited Double Cage Induction Generator, Transient Stability, Oscillation Damping, Self-Tuning Fuzzy Control, Flexible AC Transmission Systems (FACTS), Generalized Unified Power Flow Controller (GUPFC), Quasi Multi-Pulse Voltage Source Converter, Simplex Method*

Nomenclature

$\mu(i)$	Output membership function of the consequent of rule i
A	Blade impact area
$a_{1,2,3}$	Tunable gains of STFDC
b_i	Center of output membership function of the consequent of rule i
C	Equivalent capacitance of DC link of GUPFC
C_p	Dimensionless power coefficient
D	Damping coefficient of SG
E	DC link voltage of GUPFC
$e(k)$	Error at sample-k
e_d	D-axis component of stator internal generated voltage of SG
e_q	Q-axis component of stator internal generated voltage of SG
E_{ref}	Reference of GUPFC DC link voltage
i_d	D-axis component of stator current of SG
i_q	Q-axis component of stator current of SG
i_{ri}	Rotor current of i^{th} winding of SEDCIG
i_s	Stator current of SEDCIG
J	Inertia of SEDCIG
j	Square root of -1
K_D	Proportional gain of reactive power flow controller
K_{ED}	Proportional gain of DC voltage controller
K_Q	Proportional gain of real power flow controller
K_{VQ}	Proportional gain of AC voltage controller
K_w	Damping gain
L_{12}	Mutual inductance of rotor of SEDCIG
L_m	Mutual inductance of SEDCIG
L_{ri}	Leakage inductance of i^{th} rotor winding of SEDCIG
L_s	Stator leakage inductance of SEDCIG
M	Inertia constant of SG
P	Number of pole pairs of SEDCIG
P	Real power flow
P_{inji}	Injected real power of i^{th} VSC to power system
P_{lossi}	Sum of switching loss and magnetic interface

Manuscript received and revised July 2012, accepted August 2012 *Copyright © 2012 Praise Worthy Prize S.r.l. - All rights reserved*

	loss of ith VSC
P_{ref}	Reference of real power flow
$P_{transferi}$	Real power exchange of ith VSC with other VSCs
P_W	Mechanical power extracted from wind
Q	Reactive power flow
Q_{inji}	Injected reactive power of ith VSC to power system
Q_{ref}	Reference of reactive power flow
R_a	Armature resistance of SG
R_C	Common end-ring resistance of SEDCIG
R_{ri}	Rotor resistance of ith winding of SEDCIG
R_s	Stator resistance of SEDCIG
T	Time constant of stator of SG
T_D	Integral time of reactive power flow controller
T_e	Electrical torque of SEDCIG
T_E	Electrical torque of SG
T_{ED}	Integral time of DC voltage controller
T_L	Load torque of SEDCIG
T_M	Mechanical torque of SG
T_Q	Integral time of real power flow controller
T_{VQ}	Integral time of AC voltage controller
V	Bus voltage
V	Voltage vector of quasi multi-pulse VSC
V_f	Excitation winding voltage of stator of SG
V_M	Voltage vector of converter M
V_N	Voltage vector of converter N
V_q	Q-axis component of stator voltage of SG
V_{ref}	Reference of bus voltage
v_s	Stator voltage of SEDCIG
V_{sei}	Voltage of series ith VSC of GUPFC
V_{seiD}	D-axis component of series ith VSC of GUPFC
V_{seiQ}	Q-axis component of series ith VSC of GUPFC
V_{sh}	Voltage of shunt VSC of GUPFC
V_{shD}	D-axis component of shunt VSC of GUPFC
V_{shQ}	Q-axis component of shunt VSC of GUPFC
V_W	Wind speed
V_{WB}	Base wind speed
V_{WG}	Gust wind component
V_{WN}	Noise wind component
V_{WR}	Ramp wind component
w	Mechanical speed of SG
w_a	Speed of arbitrary rotating reference frame
w_B	Blade angular velocity
w_{ref}	Base mechanical speed of SG
X	Stator reactance of SG
β	Output signal of FGT
β_p	Blade pitch angle
γ	Tip speed ratio
δ	Torque angle of SG
ΔE	Error for DC link voltage controller of GUPFC
ΔP	Error for real power flow controller of GUPFC
ΔQ	Error for reactive power flow controller of GUPFC
ΔV	Error for AC voltage controller of GUPFC
$\Delta V_{q(k)}$	Output signal of FDC at sample-k
Δw	Mechanical speed error of SG
θ_{sei}	Phase angle of series ith VSC of GUPFC
θ_{sh}	Phase angle of shunt VSC of GUPFC
ρ	Air density
$\Sigma e(k)$	Error-integral at sample-k
φ_{ri}	Rotor flux linkage of ith winding of SEDCIG
φ_s	Stator flux linkage of SEDCIG

I. Introduction

Integration of large wind farms with electrical network is inevitable due to growing electrical demand and environmental reasons which leads to interconnected operation of synchronous generators and wind turbine driven generators [1],[2]. The use of induction machines in wind generation is widely accepted as a generator of choice due to their simple structure and cost [3]-[5]. On one hand, wind farms employing induction generators consume reactive power which produces low voltage profile and dynamic instability observed following after faults [6],[7]. On the other hand, the integration not only requires stable operation of synchronous generators, but also induction generators should operate stable without disturbing demand side. This situation comes into prominence since the induction generator's behavior during a fault is very different from that of a synchronous generator. Conventionally, electromechanical oscillations, either being local mode (1-2 Hz) or inter-area mode (0.2-0.8 Hz), are occurring due to the natural dynamic behavior of synchronous machines when the system is subjected to faults and may lead to total or partial power interruption if not damped out effectively [8].

Rotor speed instability of the induction generator is seen when it is subjected to a nearby fault. In this situation, the rotor may accelerate and reach higher steady-state speed [9].

Self-excited double-cage induction generators (SEDCIG) which energize the wind farm is considered in this study, due to following two reasons [3]: (i) Although, doubly fed induction generator (DFIG) has gained remarkable attention currently, SEDCIGs are still operated in many grid-connected wind turbines, (ii) the transient behavior of DFIG is similar to SEDCIG when the crowbar system of the DFIG protects the converter under grid fault by bypassing the rotor circuit over the crowbar impedance.

Combining two completely different machine stability concerns mentioned above, stability of the power systems connected with the wind farm is enhanced by generalized unified power flow controller (GUPFC), which extends power flow control of multi-lines or a sub-network rather than power flow control of a single line by unified power flow controller (UPFC) or static synchronous series compensator (SSSC) [10],[11]. In this study, the following control tasks are provided simultaneously by GUPFC, which has not been proposed before: 1) oscillation damping of power system with

Copyright © 2012 Praise Worthy Prize S.r.l. - All rights reserved

wind farm and its enhancement by a self-tuning fuzzy damping controller (STFDC), 2) multi-line real and reactive power flow control, 3) AC bus voltage control, and 4) DC link voltage control.

In this work, quasi multi-pulse converters switched at grid frequency of 60 Hz is adopted from the authors' previous work [12], in order to decrease GUPFC losses and to embed realistic converter dynamics into the simulated waveforms. The self-tuning scheme for PI type fuzzy controllers has been originally proposed by Mudi et al [13] and later applied to thyristor controlled series capacitor to improve the stability of multi-machine power systems by Hameed et al [14]. STFDC is different here with altered fuzzy inputs. The performance is further improved by optimizing scaling gains using non-gradient simplex method.

The stability concern is first evaluated for three-phase and single-phase faults without GUPFC in the power network and then with GUPFC. The dynamic simulations investigate the impact of faults (i) on the stability of synchronous/induction generators, (ii) on GUPFC performance when controlling real and reactive power flows as well as AC bus voltage. PSCAD and MATLAB are used simultaneously for simulating transient behavior of the models.

The study is structured as follows: Section 2 describes the representation of system components which generate electrical power. Section 3 deals with the operation principle of GUPFC. Section 4 describes the simulation model of the studied system from the simulation environment point of view. Section 5 designates control principles for GUPFC and introduces the proposed self-tuning fuzzy damping scheme with the simplex optimization routine. Section 6 presents and discusses the simulation results of the case studies and conclusion is given in Section 7.

II. Dynamic Equations for Power Generation

II.1. Wind Model

The wind can be modeled with the following equation that properly includes spatial effects of the wind behavior such as gusting, ramp changes, and background noise [15]:

$$V_W = V_{WB} + V_{WG} + V_{WR} + V_{WN} \tag{1}$$

where V_W is the wind speed, V_{WB} is the base or mean wind speed which is always assumed to be present where the wind generator is required to be in service. V_{WG} is the gust wind component, V_{WR} is the ramp wind component, and V_{WN} is the noise wind component. In this work, only transient fault simulations are considered where the simulated events last up to only 12.5 s. Moreover, the wind farm considered here is aggregations of many single wind turbines in which wind speed variations can cancel each other [16]-[18]. That's why natural wind variations (V_{WG}, V_{WR}, V_{WN}) are not taken into account.

V_{WB} is set to 14 m/s [16], [19] allowing all turbines to produce rated power.

II.2. Blade Dynamics

The mechanical system mainly consists of blade and shaft which transforms wind kinetic energy into rotational motion. Shaft dynamics are not presented in this study which is characterized by blade speed, hub speed, gear box speed, and the generator mechanical speed [15]. The available wind power is assumed to be captured by horizontal axis wind turbine with three blades. The blade dynamics are represented by the following functions [15]:

$$\begin{aligned} \gamma &= \frac{V_W}{w_B} \\ C_p &= \frac{1}{2}\left(\gamma - 0.022\beta_p{}^2 - 5.6\right)e^{-0.17\gamma} \\ P_W &= \frac{1}{2}\rho A C_p V_W{}^3 \end{aligned} \tag{2}$$

where w_B is the blade angular velocity, γ is the tip speed ratio, β_p is the blade pitch angle, C_p is the dimensionless power coefficient, ρ is air density, and A is blade impact area. P_W is the resultant mechanical power which is extracted from the wind. Wind turbine parameters are given in Appendix.

II.3. Self-Excited Double-Cage Induction Generator

Self-excited double cage induction generator (SEDCIG) can be modeled by the following equations for its one phase while saturation effects are ignored [20]. Underlined variables denote space vectors in the arbitrary rotating reference frame with a speed of w_a:

$$\begin{aligned} \underline{v_s} &= R_s \underline{i_s} + d\underline{\varphi_s}/dt + jw_a\underline{\varphi_s} \\ 0 &= R_{r1}\underline{i_{r1}} + d\underline{\varphi_{r1}}/dt + j\left(w_a - w\right)\underline{\varphi_{r1}} + R_c\left(\underline{i_{r1}} + \underline{i_{r2}}\right) \\ 0 &= R_{r2}\underline{i_{r2}} + d\underline{\varphi_{r2}}/dt + j\left(w_a - w\right)\underline{\varphi_{r2}} + R_c\left(\underline{i_{r1}} + \underline{i_{r2}}\right) \\ \underline{\varphi_s} &= L_s\underline{i_s} + L_m\left(ir1 + ir2\right) \\ \underline{\varphi_{r1}} &= L_{r1}\underline{i_{r1}} + L_m\underline{i_s} + L_{12}\underline{i_{r2}} \\ \underline{\varphi_{r2}} &= L_{r2}\underline{i_{r2}} + L_m\underline{i_s} + L_{12}\underline{i_{r1}} \\ T_e &= \left(3/2\right)P\underline{\varphi_s} \times \underline{i_s} \\ T_e - T_L &= \left(J/P\right)dw/dt \end{aligned} \tag{3}$$

where v, i, φ respectively describes voltage, current, and flux linkage. Subscripts r and s stands for rotor and stator, respectively. Subscripts 1 and 2 represents the rotor windings, respectively. R describes resistance and R_C is common end-ring resistance between the two cages

Copyright © 2012 Praise Worthy Prize S.r.l. - All rights reserved

in the double-cage induction machine.

L represents inductance and L_m is the mutual leakage inductance between stator and two rotor windings. L_{12} is the mutual leakage inductance between the two rotor windings. w is the rotation speed and P is the number of pole pairs. T_e and T_L stands for electrical torque and load torque, respectively. J is the inertia of the machine. The model parameters are given in Appendix.

II.4. Salient Pole Synchronous Generator (SG)

The unsaturated dq model of SG can be approximated by the following functions [21]:

Stator equations:

$$\begin{aligned}
V_q &= -R_a i_q + e''_q - X''_d i_d \\
V_d &= -R_a i_d + e''_d - X''_q i_q \\
T''_{d0}\frac{de''_q}{dt} &= e'_q - e''_q - \left(X'_d - X''_d\right) i_d \\
T'_{d0}\frac{de'_q}{dt} &= V_f - e'_q - \frac{X_d - X'_d}{X'_d - X''_d}\left(e'_q - e''_q\right) \\
T''_{q0}\frac{de''_d}{dt} &= e'_d - e''_d - \left(X'_q - X''_q\right) i_q \\
T'_{q0}\frac{de'_d}{dt} &= -e'_d - \frac{X_q - X'_q}{X'_q - X''_q}\left(e'_d - e''\right)_d \\
T' &= e''_d i_d + e''_q i_q + \left(X''_q + X''_d\right) i_d i_q
\end{aligned} \tag{4}$$

Rotor equation:

$$M\frac{d^2\delta}{dt^2} + D\frac{d\delta}{dt} = T_M - T_E \tag{5}$$

where V, i, X respectively describes voltage, current, and reactance. Subscripts d and q stands for direct and quadrature axis, respectively. Subscript 0 means open circuit and R_a describes armature resistance. T defines time constant. V_f and e is the excitation winding voltage and internal generated voltage, respectively. Superscripts ' and " respectively denotes transient and sub-transient modes. M and D describes inertia constant and damping coefficient, respectively. T_E is electrical torque which is opposing the mechanical torque, T_M. δ is the torque angle. The model parameters are given in Appendix.

III. Principle of GUPFC

The simplest power circuit configuration of GUPFC consisting of three voltage source converters (VSC) is schematically drawn in Fig. 1(a). The shunt converter (VSC1) is connected to Bus i through shunt coupling transformer (Tr1). The two series converters (VSC2-3) are coupled to the transmission lines (Line m-n) through series transformers (Tr2-3), respectively. When switch S1 is on and switches S2 and S3 are off, GUPFC is in full control mode in which each converter can synthesize three-phase controllable voltage both in magnitude (V_{sh}, $V_{se1\text{-}2}$) and phase angle (θ_{sh}, $\theta_{se1\text{-}2}$) with independent reactive power injection ($Q_{inj1\text{-}3}$) capability. Real and reactive power injections of each converter to the power network are shown in Fig. 1(b). DC link with equivalent capacitance C enables real power exchange ($P_{transfer1\text{-}3}$) between converters so that sum of real power injections ($P_{inj1\text{-}3}$) from converters into grid is zero. $P_{loss1\text{-}3}$ is the sum of switching loss and coupling transformer loss of each converter, respectively. The power equations are defined in (6) where loss meeting function of GUPFC is assigned to shunt converter:

$$\begin{aligned}
&P_{inj1} - P_{transfer1} - P_{loss1} - P_{loss2} - P_{loss3} = 0 \\
&P_{inj2} - P_{transfer2} = 0 \\
&P_{inj3} - P_{transfer3} = 0 \\
&P_{transfer1} + P_{transfer2} + P_{transfer3} = 0
\end{aligned} \tag{6}$$

Each converter of GUPFC is designed as quasi multi-pulse converter in authors' previous work [12] by joining two quasi 24-pulse converter units (converter M-N), connected in parallel through a common DC link with a capacitance of C=0.2 F. Coupling transformers Tr1-3, which are conceptually shown in Fig. 1(a), are designed as special magnetic interfaces so that the AC output voltages of converter M and N are added with desired phase shifts to obtain controllable voltage for quasi multi-pulse converter. In total, 144 gate turn-off thyristors (GTO) with 144 reverse-parallel diodes are employed in GUPFC and each GTO is triggered only once in fundamental cycle of 60 Hz which significantly reduces converter losses. Moreover harmonic content is similar to that of true multi-pulse converter with equal number of switching devices and the use of quasi multi-pulse GUPFC model is more accurate than existing low-order, average or functional models.

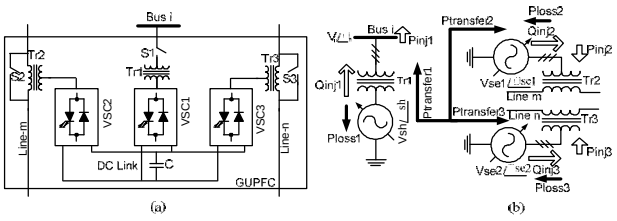

Figs. 1 Schematic representation of GUPFC: (a) Converter arrangement (b) Real/reactive power interaction with the system

IV. Power system Configuration

Time domain simulation studies are carried out on wind farm integrated power system installed with GUPFC, which is shown in Fig. 2. The system is kept as simple as possible and grid data are inspired from IEEE first benchmark model [22]. Series converters VSC2 and

Copyright © 2012 Praise Worthy Prize S.r.l. - All rights reserved

VSC3 are inserted into Line-2 and Line-1, respectively. Shunt converter (VSC1) is connected to Bus-1. The wind farm rated at 50 MVA is comprised of 20 SEDCIGs operating coherently, each driven by a horizontal axis three-blade wind turbine. 320 uF capacitor for each phase is installed at wind farm bus for unity power factor operation. AC grid power generation side is the aggregated model of 5 parallel hydro-governed SGs with solid-state exciters, rated at 120 MVA each. 100 MVA and 154 kV are chosen as base values and start-up transients of the generators are not taken into account since the faults are considered soon after the system comes to steady-state.

Test power system including wind farm and GUPFC with three-converters and control blocks have all been modeled in PSCAD while fuzzy interfaces are designed in MATLAB fuzzy logic toolbox. PSCAD is interfaced with MATLAB through a custom written interface in PSCAD [23]. In this study, an interface that calls a MATLAB m-file has been formed like in Fig. 2, which calls the fuzzy systems from MATLAB engine through FORTRAN script. PSCAD exchanges data with MATLAB continuously at every solution time step of 50 μs.

V. GUPFC control

GUPFC shown in Fig. 1(a) can control Bus-i voltage, as well as real and reactive power flows of Line-m and Line-n, respectively. The control scheme for shunt and series converters is based on the decomposition of converter voltage vectors (V_{se1},V_{se2},V_{sh} in Fig. 1(b)) into direct and quadrature axis (D,Q) components [12]. Real and reactive power flows can be controlled by series converters using PI controllers:

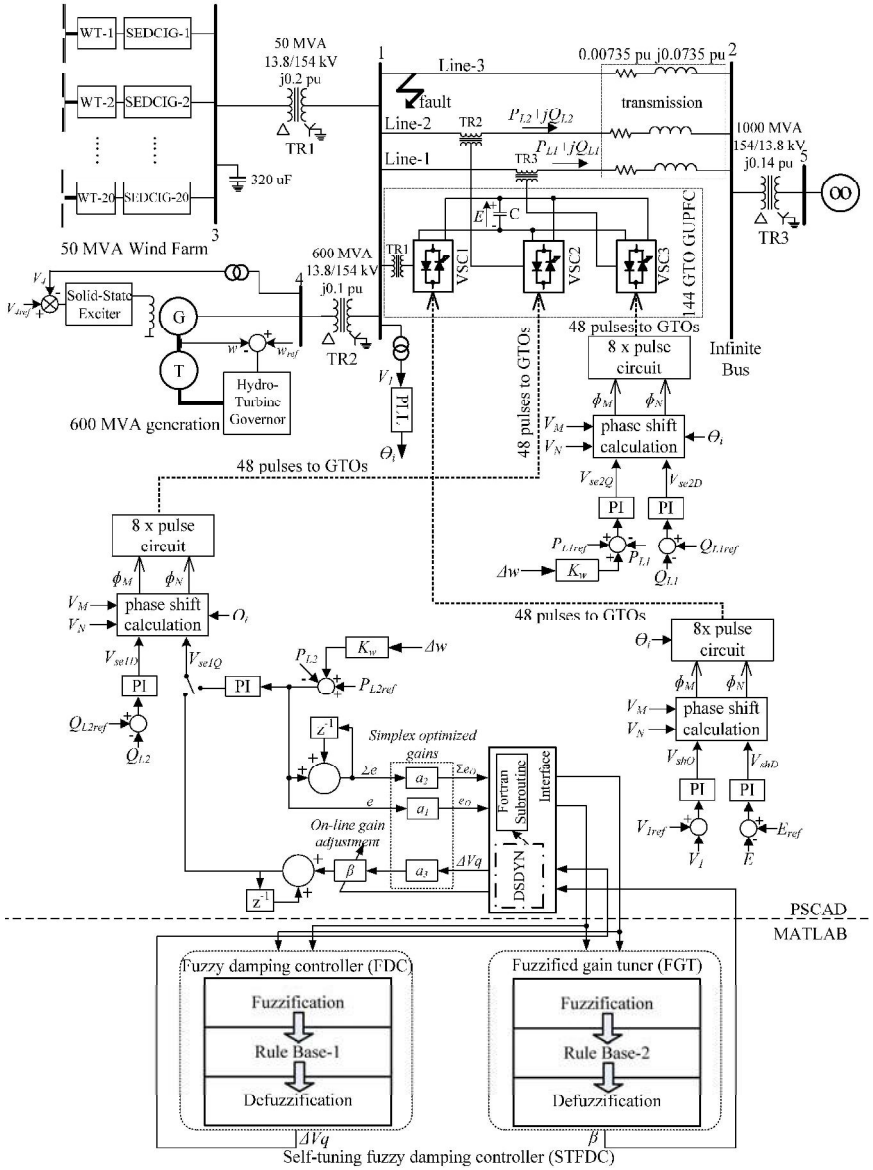

Fig. 2. Power system configuration embedded with GUPFC and the proposed damping scheme

Copyright © 2012 Praise Worthy Prize S.r.l. - All rights reserved

$$V_{seiD} = \left(K_{Di} + 1/T_{Di}s\right)\Delta Q$$
$$V_{seiQ} = \left(K_{Qi} + 1/T_{Qi}s\right)\Delta P \quad (7)$$

DC link voltage of GUPFC and Bus-i voltage can be controlled by the shunt converter using PI controllers:

$$V_{shQ} = \left(K_{VQ} + 1/T_{VQ}s\right)\Delta V$$
$$V_{shD} = \left(K_{ED} + 1/T_{ED}s\right)\Delta E \quad (8)$$

In (7) and (8), i=1,2, K is the proportional gain, and T is the integral time. $\Delta P=(P_{ref}-P)$ and $\Delta Q=(Q_{ref}-Q)$ is the real and reactive power flow error, respectively. $\Delta E=(E_{ref}-E)$ and $\Delta V=(V_{ref}-V)$ stands for error in DC link voltage and error in AC bus voltage, respectively. Once the required DQ-axis voltage components for each converter are obtained from (7) and (8), required phase shifts (α, δ) to the voltages of converter M and N ($\vec{V}_M$,$\vec{V}_N$) can be derived in (9), according to Fig. 3:

$$\alpha = tan^{-1}\left[\frac{\left(V_M + V_N\right)^2 - \left(V_D\right)^2 - \left(V_Q\right)^2}{\left(V_D\right)^2 + \left(V_Q\right)^2}\right]^{1/2}$$
$$\delta = tan^{-1}\frac{V_Q}{V_D} \quad (9)$$

Here the idea is to get voltage vector $\vec{V}$ for each converter by adding $\vec{V}_M$ and $\vec{V}_N$ for quasi multi-pulse operation. Pulse generating circuit for each six-pulse converter is also presented in Fig. 3.

In case of damping mode, real power flow control loop in (7) is removed and the error at sample-k is simply modified by an auxiliary damping signal based on the speed error of SG ($\Delta w=w_{ref}-w$). In this case error at sample-k becomes:

$$e(k) = \Delta P + K_w \Delta w \quad (10)$$

where K_w is the damping gain. Since aggregated synchronous machine model is used, w and w_{ref} represents the speed at sample-k, and base speed of all parallel operating generators, respectively. As opposed to one of the originally proposed fuzzy inputs in [13], control system is made insensitive to noise in the error measurement using error-integral instead of error-derivative which lessen control signal oscillations highly observed in simulation cases. In this case, the error-integral at sample-k can be computed as:

$$\Sigma e(k) = \Sigma e(k-1) + e(k) \quad (11)$$

It is important to note that the series converter, where STFDC is not utilized controls real power flow on Line-1 using (7) with auxiliary damping signal. The proposed damping scheme is based on a robust self-tuning PI-type fuzzy controller [13] and constructed from a fuzzy damping controller (FDC) which operates with a fuzzified gain tuner (FGT) concurrently as shown in Fig. 2.

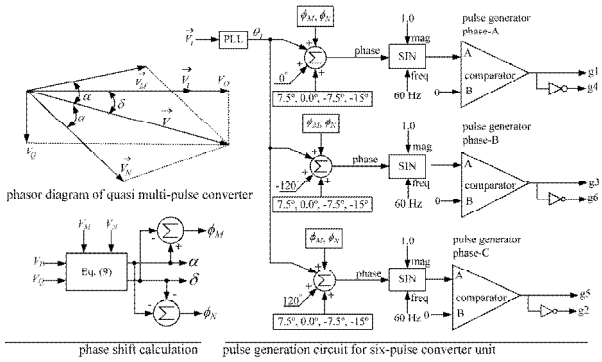

Fig. 3. Phase shift calculation and pulse generation blocks [12]

V.1. *Fuzzy Damping Controller* (*FDC*)

In FDC, the signals e and Σe in (10) and (11) are respectively multiplied by gains (a_1, a_2), which needs to be optimized. Crisp values are then mapped to their equivalent fuzzy values by the membership functions of Knowledge Base in Fig. 4. Membership functions for e_O and Σe_O are symmetrical triangles (except the two at both ends) which have equal 50% base overlap, divides the domain [-1,1] into 7 equal regions. The term sets of e_O and Σe_O contains the same linguistic expressions for the magnitude part of the linguistic values and characterizes Rule Matrix-1 in Fig. 4 which contains 49 rules. The cell defined by the intersection of the first row and the first column represents a rule such as, {"If Σe_O is P1 and e_O is N2 then ΔVq is N1"}. The antecedents are evaluated by applying "*min*" operator and the output fuzzy set is truncated by applying "*min*" implication operator. The fuzzy sets are aggregated into a single fuzzy set by "*max*" operator that should be later dezuffied to resolve a single real number for each output variable. Centroid defuzzification method is applied to get incremental change in series converter voltage as follows:

$$\Delta V_q(k) = \frac{\sum_{i=1}^{49} b_i \int \mu(i)}{\sum_{i=1}^{49} \int \mu(i)} \quad (12)$$

where $\mu(i)$ and b_i is the output membership function and the center of output membership function of the consequent of rule i, respectively. Finally, at sample-k, q-axis component of the series converter voltage for oscillation damping and as well as for dynamic real power flow control is calculated in (13) where β is the value of gain factor at sample-k which is decided by FGT:

$$V_q(k) = V_q(k-1) + a_3 \beta \Delta Vq(k) \quad (13)$$

Copyright © 2012 Praise Worthy Prize S.r.l. - All rights reserved

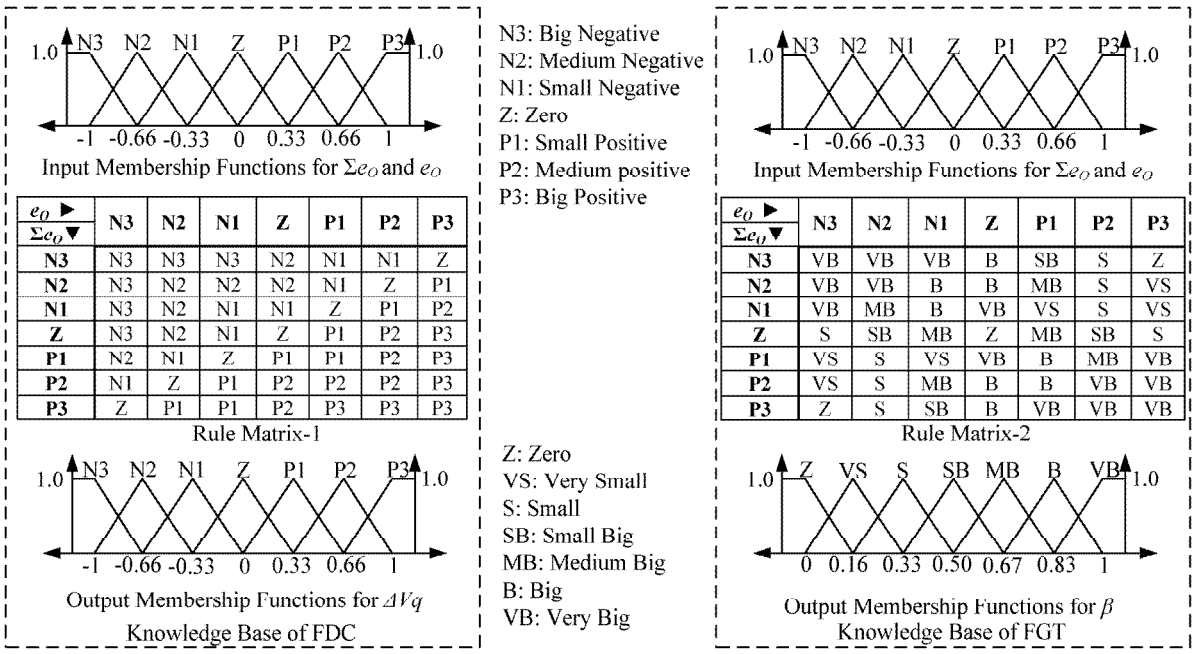

Fig. 4. Membership functions and fuzzy rules for STFDC

V.2. Self-Tuning Fuzzy Damping Controller (STFDC)

In STFDC scheme, FDC performance is further enhanced by FGT which computes the gain factor β by a self-tuning mechanism independent from FDC itself. So, two fuzzy modules (FDC and FGT) operate concurrently to generate *Vq* signal reference for the series converter. The value of β is not fixed and modified at each sample-*k* according to the following relation:

$$\beta(k) = f\left(e_o(k), \Sigma e_o(k)\right) \tag{14}$$

where *f* denotes a non-linear mapping function, described by Rule Matrix-2 with 49 rules in Fig. 4 and associated by the FGT scheme whose structure is exactly the same for its fuzzy operators and input membership functions with those of FDC. Universe of discourse for β lies in the domain [0,1] and is obtained by shifting and scaling (add 1 and multiply with 0.5) input membership functions of FDC along the horizontal axis. Rule Matrix-2 is designed to improve the damping performance of GUPFC under large disturbances such as three-phase short circuit on transmission lines. For instance, after a fault occurs, error may be small-positive (P1) but error-integral can be sufficiently large (P3). In this case, β should be big enough (VB) to increase converter voltage. Under such a situation, the rule is {"If Σe_O is P3 and e_O is P1 then β is VB"}.

V.3. Tuning of Scaling Factors

The scaling factors (a_1, a_2, and a_3) are used to normalize input variables of the FDC. {$e_O=a_1e$; $\Sigma e_O=a_2\Sigma e$}. Similarly, FDC output variable (ΔV_q) is first multiplied by a_3 then tuned by FGT adaptively. Commonly, there is no well-defined method for selection of scaling factors [13]. In this study, these parameters are optimized by nonlinear-simplex method of Nelder and Mead, which is a non-gradient search algorithm based on a figure called "simplex" [24]. This method runs along vertices of the simplex defined by the number of tuning variables (in this case 3) to find the minimum value of a fitness function.

The worst vertex is defined where the function is the largest, is rejected and replaced by a new vertex. A new simplex is generated until the values of the function at the vertices are the smallest. Simplex size is then reduced iteratively until the coordinates of the optimal solution are found. The fitness function for finding the optimal values of scaling factors is based on integral time absolute error (ITAE) and given in (15):

$$f(a_1, a_2, a_3) = \int_{t=t_0}^{T} \left(t \cdot |w_b - w|\right) \cdot dt \tag{15}$$

where *t* is the simulation time, t_0 is the fault time. *T* is the total simulation time for Case 1 described in Section *VI. 1*. In this approach, the optimization algorithm is given control to perform several consecutive runs with a view to minimize *f*, which is computed from the results of each simulation run [25]. The flow chart of the algorithm and its convergence performance are shown in Figs. 5.

The value of *f* is minimized from 0.072 to 0.0114 in 51 iterations for a tolerance of 1.0E-6. PSCAD becomes fitness function evaluator while FDC is executed by MATLAB and FGT is deactivated. The optimization results are listed in Table I.

Copyright © 2012 Praise Worthy Prize S.r.l. - All rights reserved

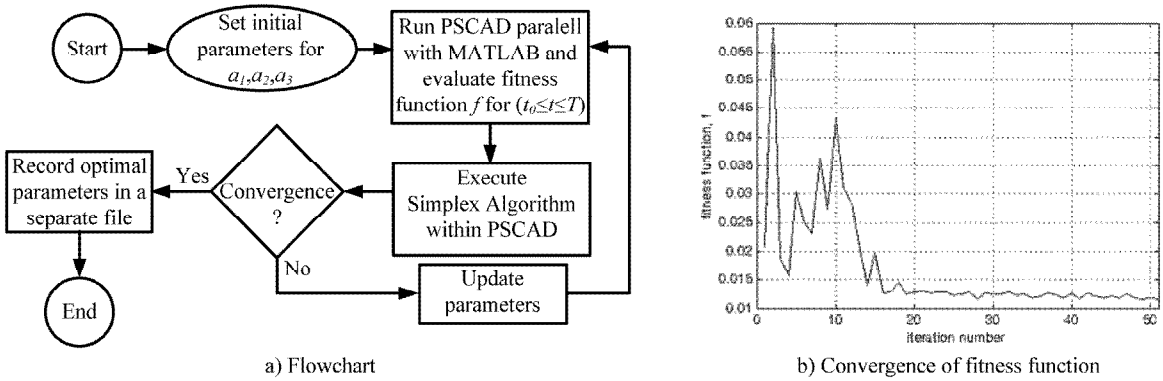

a) Flowchart b) Convergence of fitness function

Figs. 5. Optimization/transient simulation interface diagram

TABLE I
OPTIMIZATION RESULTS OF SCALING FACTORS

scaling factors	a_1	a_2	a_3
initial guess	0.001	0.001	0.001
converged result	0.7369	0.3253	0.8221

VI. Case studies

The performance of STFDC is examined for different disturbance conditions in conjunction with the following dynamic control tasks of the GUPFC:

- Line-2 real power flow (P_{L2}) control using either FDC or STFDC by VSC2
- Line-2 reactive power flow (Q_{L2}) by VSC2 using (7)
- Line-1 real power flow (P_{L1}) by VSC3 using (8)
- Line-1 reactive power flow (Q_{L1}) by VSC3 using (7)
- Bus-1 voltage (V_1) control by VSC1 using (7)
- DC link voltage (E) control by VSC1 using (7)

VI.1. Case 1

A three-phase fault of 120 ms duration is applied to Line-3 near Bus-1 at 8.5s. Pre-disturbance operating conditions are; P_{L1}^{ref}=1.75 pu, P_{L2}^{ref}=0.5 pu, Q_{L1}^{ref}=Q_{L2}^{ref}=0.0 pu, E^{ref}=2.0 kV, and V_1^{ref}=1.0 pu. To have a quantitative comparison, the ITAE values between 8.5 s and 12.5 s have been calculated for different control schemes.

Although, STFDC is only activated for VSC2 and Line-2 reactive power flow and Line-1 real and reactive power flows are controlled by simple PI regulators, it is found that STFDC indirectly smoothens the variations of simulated waveforms against fault and shows better performance than FDC in general. As evidence by response curves depicted in Fig. 6(a), STFDC performance is superior to FDC on SEDCIG rotor speed damping, being also better than that of PI controller.

In Fig. 6(b), STFDC responses better than FDC and PI controller in damping SG oscillations with reduced undershoot/overshoot and less settling time. As the consequence of the fault, real and reactive power flow variations of Line-1, presented in Figs. 6(c)-(d), and those of Line-2 presented in Figs. 6(e)-(f) are minimized better by STFDC with less undershoot/overshoot compared to the FDC.

DC link voltage excursions of GUPFC for different damping control schemes are depicted in Fig. 6(g) and it is found that among the two control schemes, the ITAE index is smaller for STFDC.

In Fig. 6(h), PI controller settles Bus-1 voltage to its controlled value of 1.0 pu with a smaller ITAE value in case of STFDC. Effect of employing STFDC with optimized gains improves transient responses of both SEDCIG speed and IG speed.

This situation is illustrated on Figs. 6(i)-(j), respectively. Voltage and current signals of the quasi multi-pulse converters after the fault are presented in Fig. 7. In more detail, simulated phase shift angles (ϕ_M and ϕ_N in Fig. 3) and selected GTO terminal voltages of the converters are shown in Fig. 8 for this case study.

VI.2. Case 2

The same fault is applied as in Case 1 to Line-3 with an increased duration of 160 ms. Pre-disturbance operating conditions are changed as; P_{L1}^{ref}=0.8 pu, P_{L2}^{ref}=1.5 pu, Q_{L1}^{ref}=Q_{L2}^{ref}=0.0 pu, E^{ref}=2.0 kV, and V_1^{ref}=1.0 pu. As shown in Fig. 9(a), longer fault results in a speed increase of SEDCIGs without GUPFC (steady-state speed is 1.483 pu which is not shown), making wind farm unstable in its operation [9].

STFDC damps speed fluctuation of SEDCIG slightly better than FDC or PI controller with less overshoot characteristics. On the other hand, Fig. 9(b) shows that STFDC exhibits good damping response to SG speed oscillations as compared to the FDC or PI controller with less settling time and less undershoot characteristics. It is observed that for both case1 and case2, SEDCIGs and SGs get stabilized and regain their original speed after fault clearance efficiently by functioning the proposed STFDC. The variations of real and reactive power flows of Line-1 shown in Figs. 9(c)-(d) and the variation of reactive power flow of Line-2 in Fig. 9(f) are indirectly improved by appointing STFDC generally with better control characteristics than FDC.

Copyright © 2012 Praise Worthy Prize S.r.l. - All rights reserved

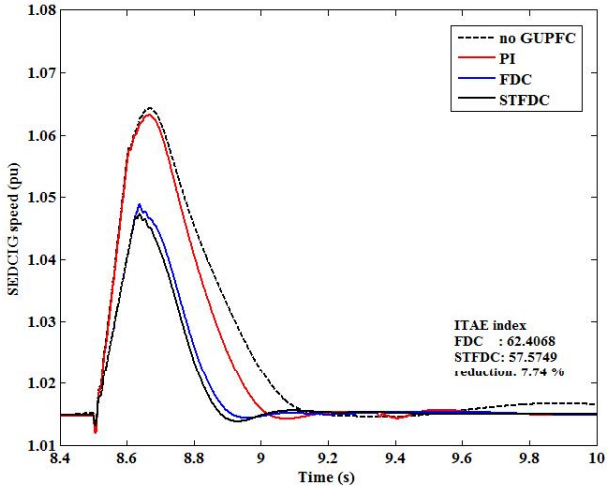

Fig. 6(a) Transient response of SEDCIG speed without GUPFC and with GUPFC under different control modes

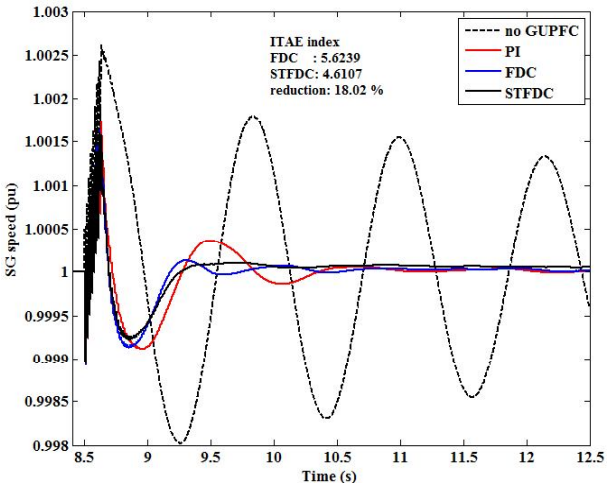

Fig. 6(b). Transient response of SG speed without GUPFC and with GUPFC under different control modes

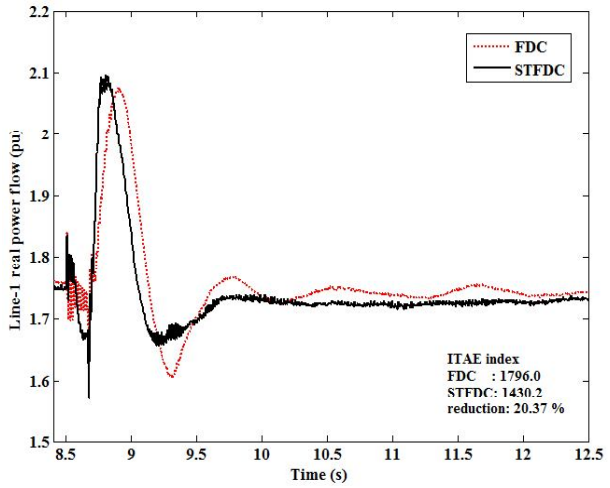

Fig. 6(c). Variation of Line-1 real power flow under different control modes following three-phase fault

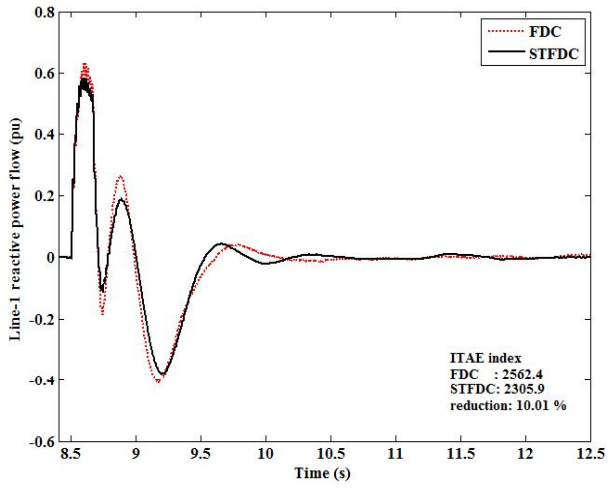

Fig. 6(d). Variation of Line-1 reactive power flow under different control modes following three-phase fault

When a comparison between Figs. 9(c) and (e) is made particularly, STFDC better holds real power flow of Line-2 in its reference value than that of Line-1, since STFDC commands the series converter which is inserted into Line-2, while only PI controller is activated for the series converter inserted into Line-1. DC voltage excursions of GUPFC depicted in Fig. 9(g) are practically the same in case of both FDC and STFDC.

Fig. 9(h) shows that the Bus-1 voltage settles down to 0.7 pu and comes to 1.0 pu steadily, practically the same response for both FDC and STFDC, but with improved ITAE index in case of STFDC. Real and reactive power fluctuations of the wind farm and AC grid under two control modes are shown in Figs. 10 and Figs. 11, respectively. STFDC mitigates these fluctuations effectively which overcomes the instability of PI controller.

In particular, Figs. 10 show that without STFDC, the reactive power demand of the wind farm is very high due to the fault, which reduces substantially once the STFDC is activated instead of PI controller.

It can be inferred that for a specific wind condition, the operation of conventional wind farm employing simple SEDCIGs can be made stable by a GUPFC with STFDC scheme.

VI.3. Case 3

The system is subjected to phase-A to ground fault on Line-3 near Bus-1 for a duration of 265 ms at 8.5 s. Pre-disturbance operating conditions are changed as; P_{L1}^{ref}=1.0 pu P_{L2}^{ref}=0.75 pu, Q_{L1}^{ref}=Q_{L2}^{ref}=0.0 pu, E^{ref}=2.0 kV, V_1^{ref}=1.0 pu. Figs. 12(a)-(b) shows the transient fluctuations of the SEDCIG speed and SG speed, respectively and provide a comparison between the different control schemes.

Besides, rise time and settling time of FDC and STFDC is practically the same for both generators, STFDC gives lower undershoot in case of SEDCIG and quantitative comparison shows better STFDC results for oscillation damping of SG speed.

Copyright © 2012 Praise Worthy Prize S.r.l. - All rights reserved

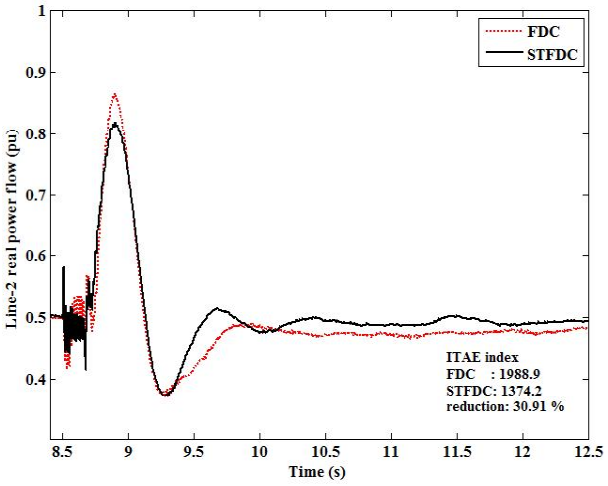

Fig. 6(e). Variation of Line-2 real power flow under different control modes following three-phase fault

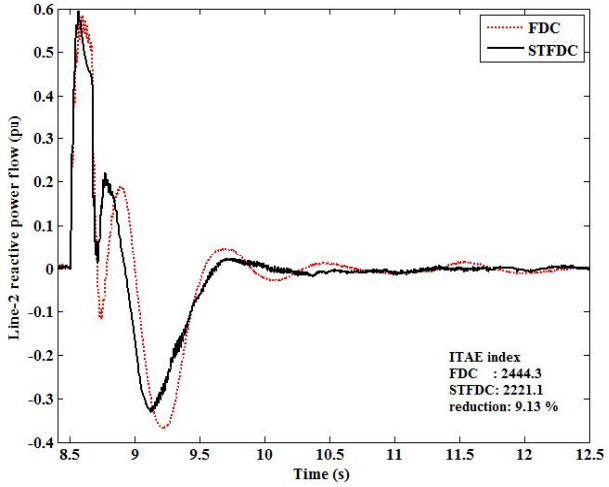

Fig. 6(f). Variation of Line-2 reactive power flow under different control modes following three-phase fault

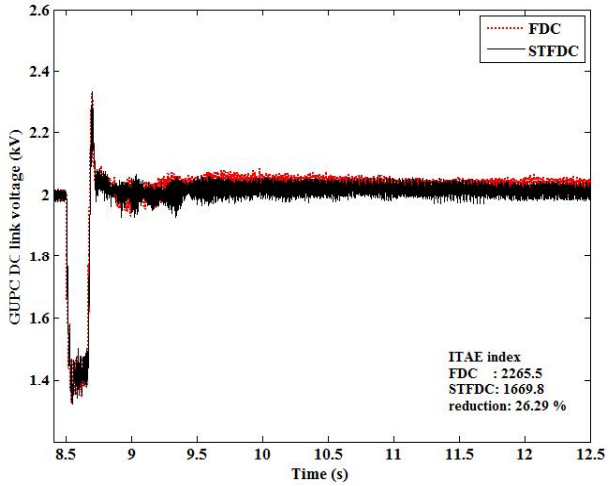

Fig. 6(g). DC voltage excursions of GUPFC under different control modes following three-phase fault

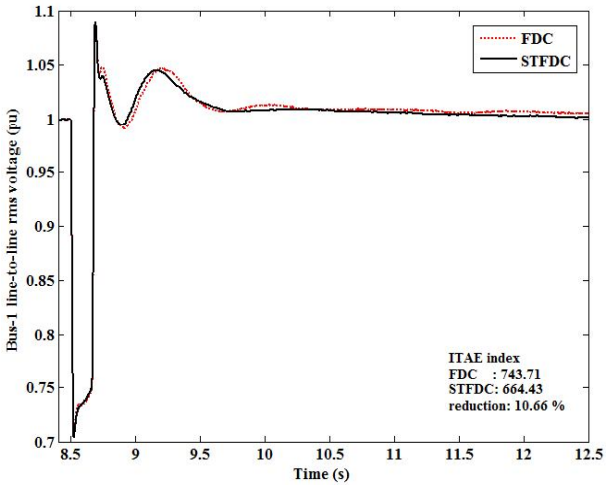

Fig. 6(h). Variation of Bus-1 voltage following three-phase fault

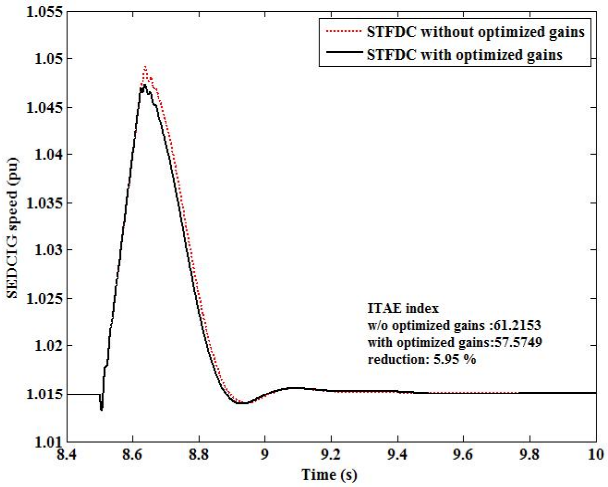

Fig. 6(i). Effect of optimized gains on transient response of SEDIG speed to three-phase fault

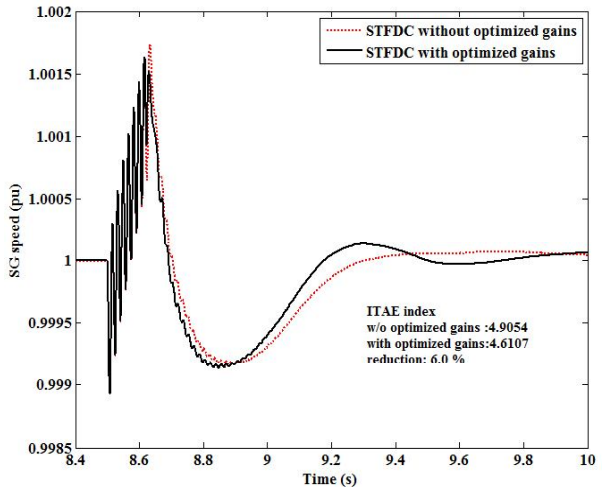

Fig. 6(j). Effect of optimized gains on transient response of SG speed to three-phase fault

Copyright © 2012 Praise Worthy Prize S.r.l. - All rights reserved

The waveforms in Figs. 12(c)-(f) indicate that STFDC is again found to be superior to FDC in general when controlling real and reactive power flows of the lines after the fault both with reduced overshoot/undershoot characteristics and with smaller ITAE indices.

Although the undershoot in case of STFDC exceeds the undershoot in case of FDC by approximately 4.5% in Fig. 12(e), the steady-state error is more effectively minimized by STFDC and a minimum ITAE index is reached. DC voltage regulation of the GUPFC is satisfactory in Fig. 12(g) and STFDC reduces DC voltage fluctuations significantly better than FDC. Fig. 12(h) shows Bus-1 voltage variations following single-phase to earth fault. The AC voltage controller is again satisfactory like in previous case studies and gives practically the same response in case of FDC and STFDC. But the performance of the AC voltage control loop is indirectly improved by STFDC with a better ITAE index than that of FDC.

VI.4. Discussion of the Simulation Results

The newly proposed damping controller is robust to change in fault type and fault duration as well as robust to changing operating conditions of the power system. Better damping characteristics for SG are achieved by GUPFC equipped with STFDC. Furthermore, STFDC can control SEDCIG speed better than FDC in case of a fault although SEDCIG speed signal is not measured in the proposed damping control scheme.

The successful operation of the shunt and series converters of the GUPFC is proved by maintaining constant DC link voltage and after faults GUPFC shows stable operation and able to restore real and reactive power flows of the transmission lines to their regulated values with significantly less variations in case of STFDC. This situation can claim longer transient fault duration that the system can withstand. It is also noted that shunt reactive support of GUPFC improves voltage profile of the wind farm bus during transient conditions.

VI.5. Harmonic Content

Table II summarizes voltage distortions at Bus-1 and Bus-2 as a measure of total harmonic distortion (THD), which are given as a ratio with respect to the fundamental component. Records of the simulated cases taken at 8.4 s (for pre-fault condition) and 12.5 s (for post-fault condition) show that THD values are within acceptable limits when STFDC is activated [26]. Hence, neither passive nor active filter is required for harmonic reduction at the ac terminals of the converters though GTOs are switched at line frequency of 60 Hz.

TABLE II
THD VALUES OF POWER SYSTEM BUS VOLTAGES

	Time	THD for $V_{1(L\text{-}L)}$	THD for $V_{2(L\text{-}L)}$
Case 1	8.4 s	1.37 %	1.57 %
	12.5 s	1.25 %	1.26 %
	Time	THD for $V_{1(L\text{-}L)}$	THD for $V_{2(L\text{-}L)}$
Case 2	8.4 s	1.37 %	1.57 %
	12.5 s	1.29 %	1.53 %
	Time	THD for $V_{1(L\text{-}L)}$	THD for $V_{2(L\text{-}L)}$
Case 3	8.4 s	1.37 %	1.57 %
	12.5 s	1.27 %	1.48 %

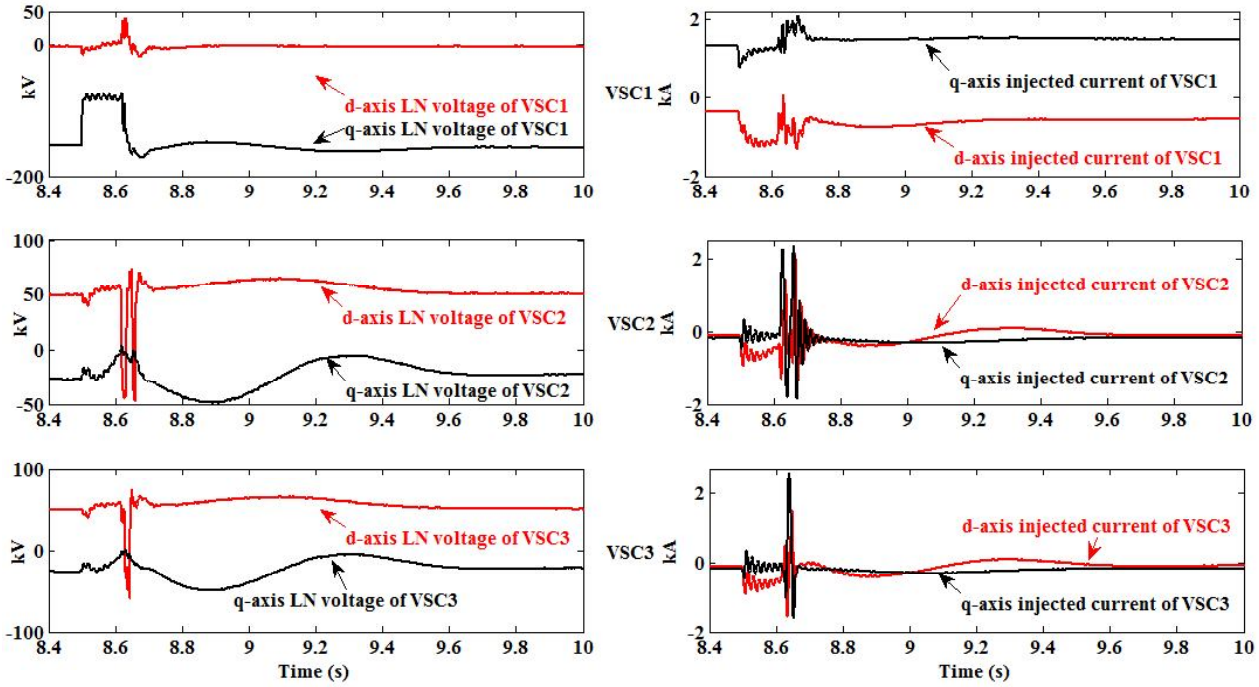

Fig. 7. Simulated voltage and curent waveforms of GUPFC converters following three-phase fault

Copyright © 2012 Praise Worthy Prize S.r.l. - All rights reserved

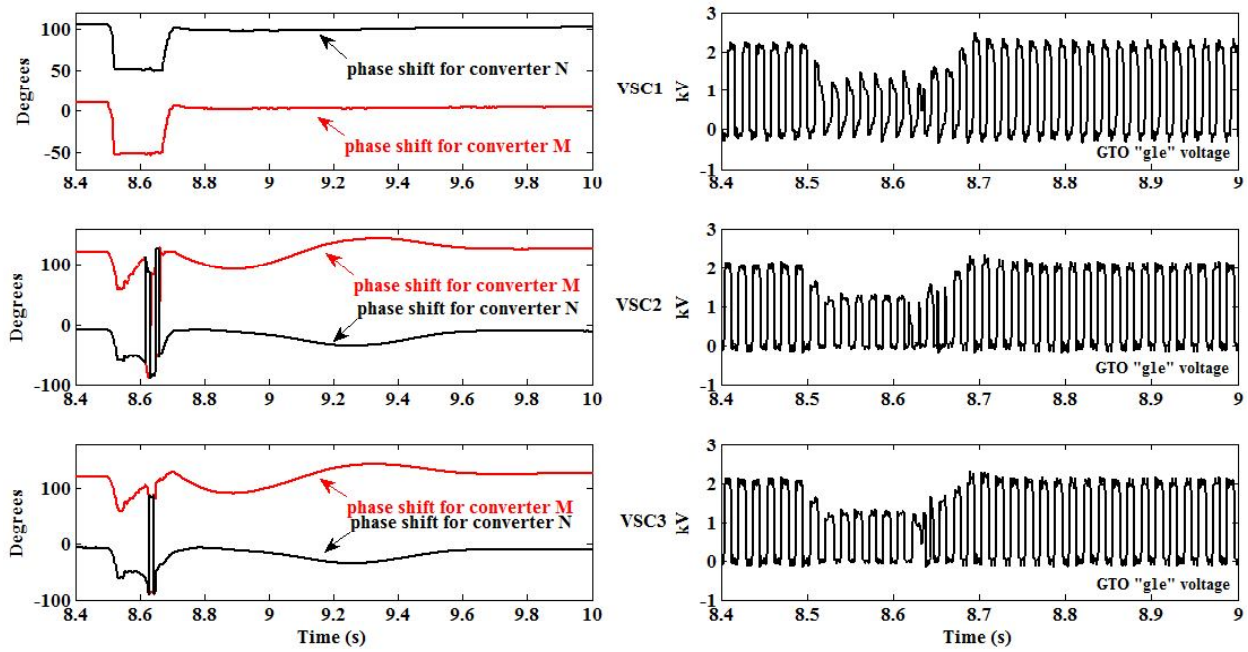

Fig. 8. Simulated phase shift angles (ϕ_M and ϕ_N) and selected GTO terminal voltages of GUPFC converters following three-phase fault

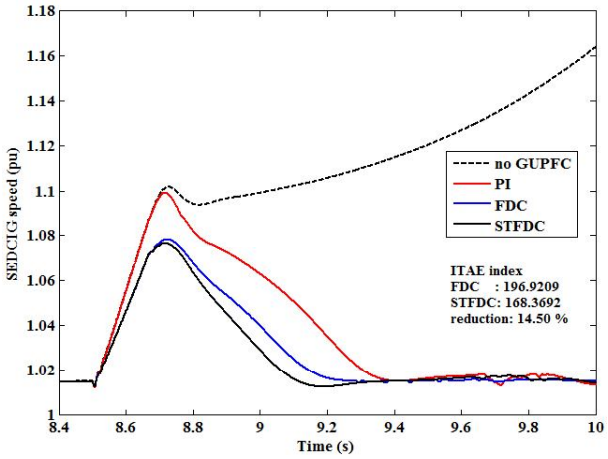

Fig. 9(a). Transient response of SEDCIG speed without GUPFC and with GUPFC under different control modes

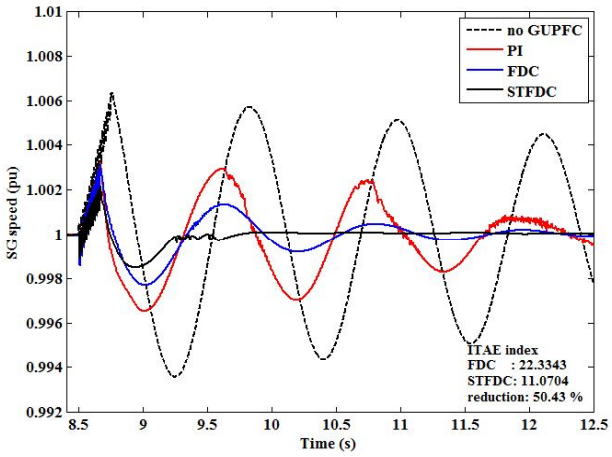

Fig. 9(b). Transient response of SG speed without GUPFC and with GUPFC under different control modes

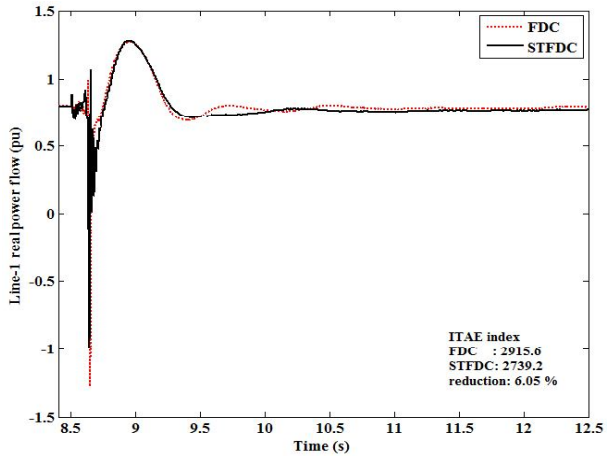

Fig. 9(c). Variation of Line-1 real power flow under different control modes following three-phase fault

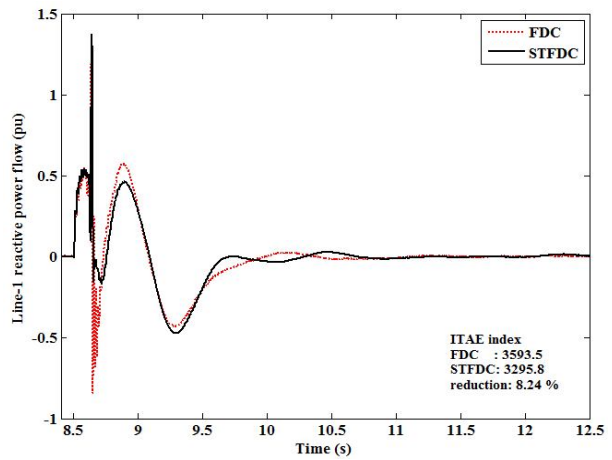

Fig. 9(d). Variation of Line-1 reactive power flow under different control modes following three-phase fault

Copyright © 2012 Praise Worthy Prize S.r.l. - All rights reserved

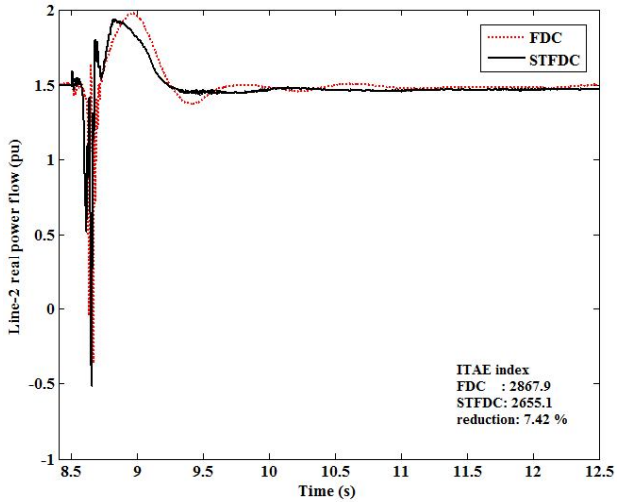

Fig. 9(e). Variation of Line-2 real power flow under different control modes following three-phase fault

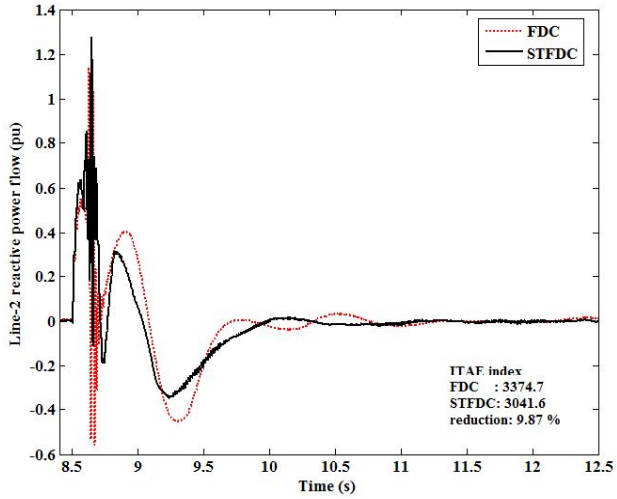

Fig. 9(f). Variation of Line-2 reactive power flow under different control modes following three-phase fault

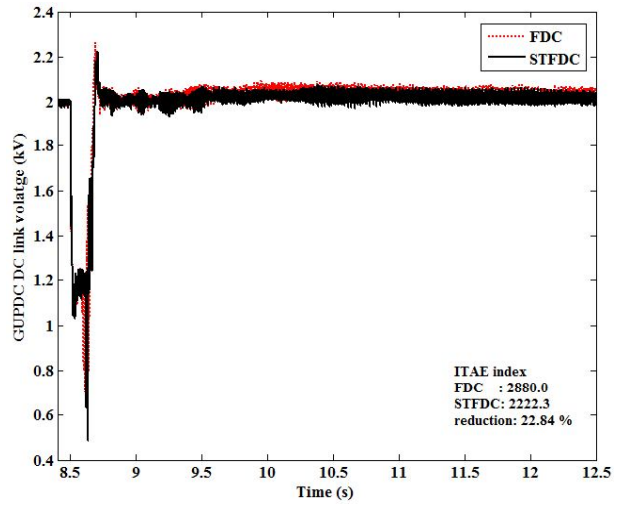

Fig. 9(g). DC voltage excursions of GUPFC under different control modes following three-phase fault

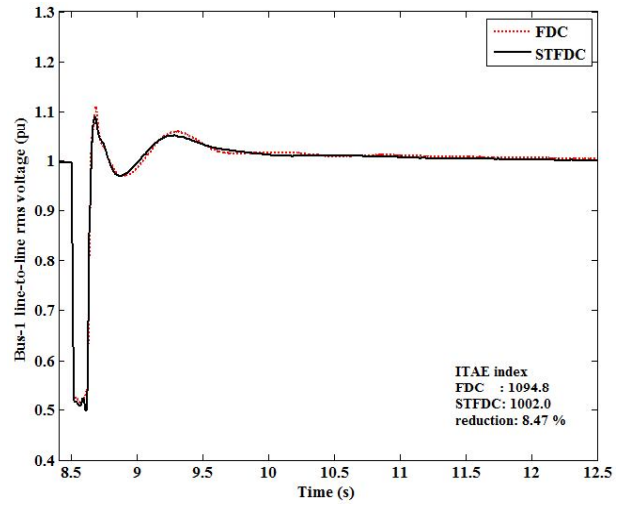

Fig. 9(h). Variation of Bus-1 voltage following three-phase fault

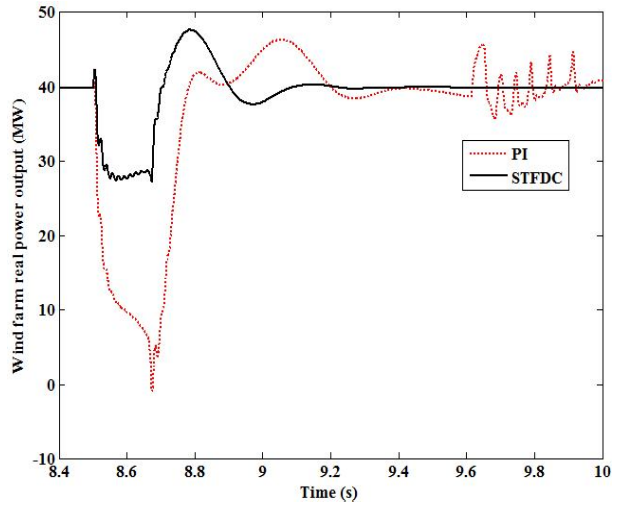

Fig. 10(a). Real power output of the wind farm following three-phase fault

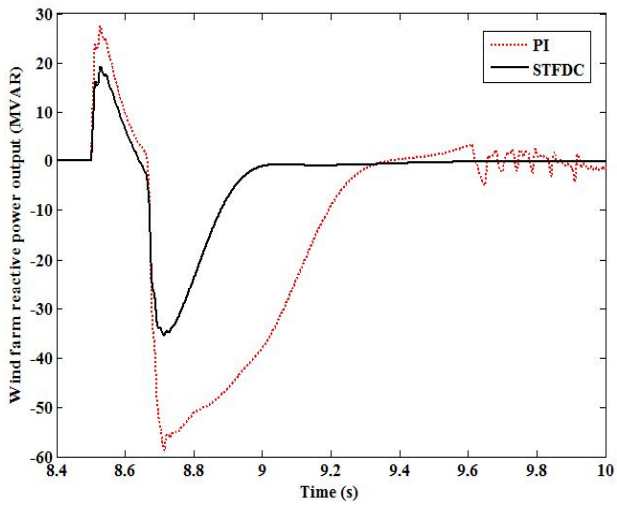

Fig. 10(b). Reactive power output of the wind farm following three-phase fault

Copyright © 2012 Praise Worthy Prize S.r.l. - All rights reserved

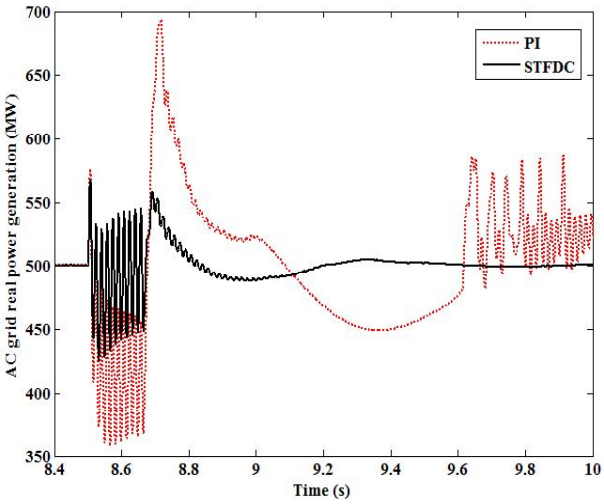

Fig. 11(a). Real power output of the SGs following three-phase fault

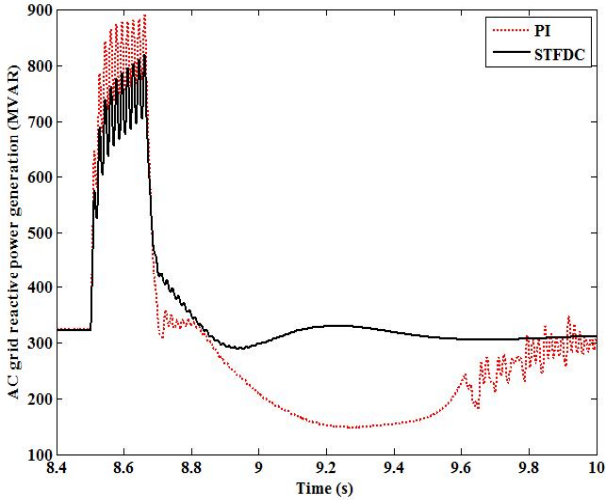

Fig. 11(b). Reactive power output of the SGs following three-phase fault

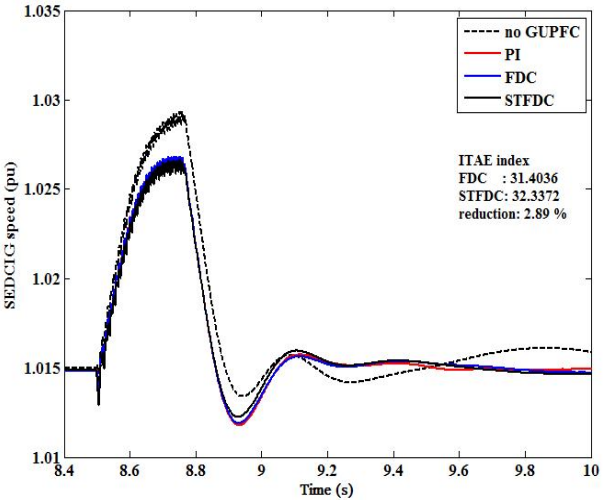

Fig. 12(a). Transient response of SEDCIG speed without GUPFC and with GUPFC under different control modes

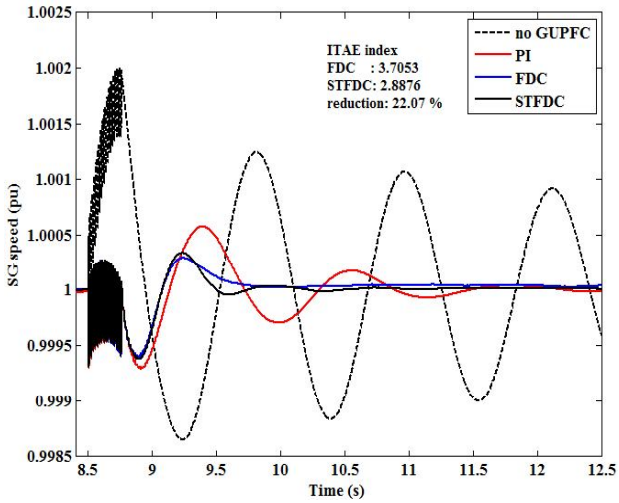

Fig. 12(b). Transient response of SG speed without GUPFC and with GUPFC under different control modes

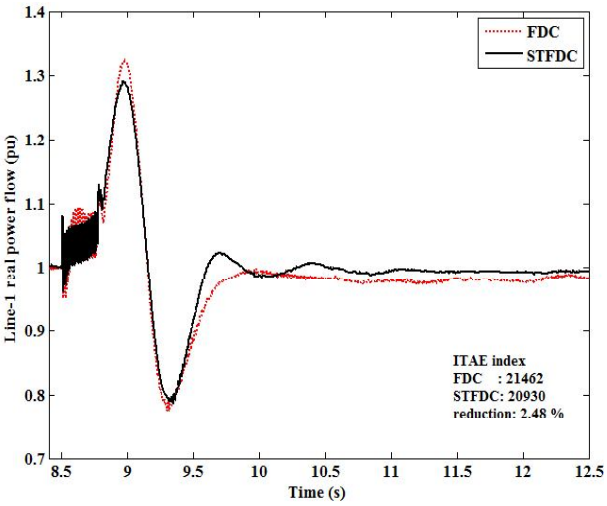

Fig. 12(c). Variation of Line-1 real power flow under different control modes following single-phase fault

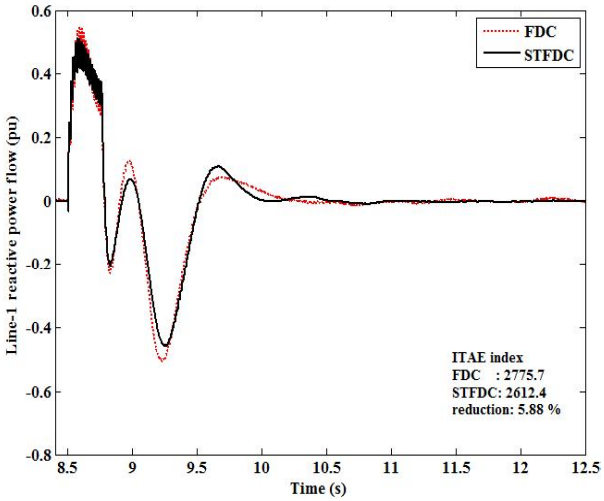

Fig. 12(d). Variation of Line-1 reactive power flow under different control modes following single-phase fault

Copyright © 2012 Praise Worthy Prize S.r.l. - All rights reserved

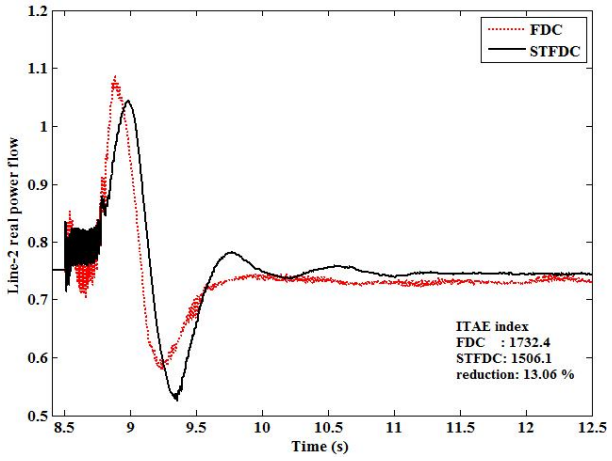

Fig. 12(e). Variation of Line-2 real power flow under different control modes following single-phase fault

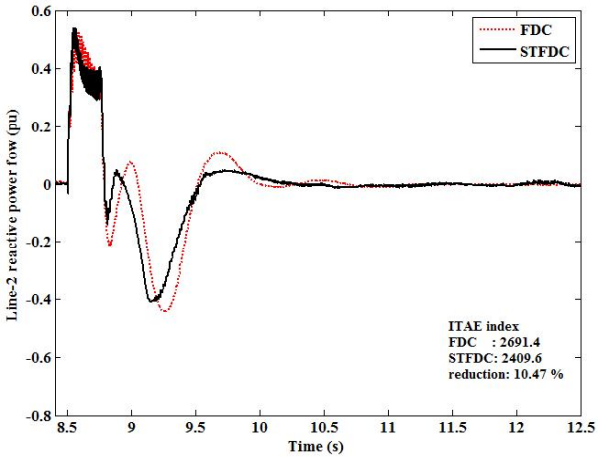

Fig. 12(f). Variation of Line-2 reactive power flow under different control modes following single-phase fault

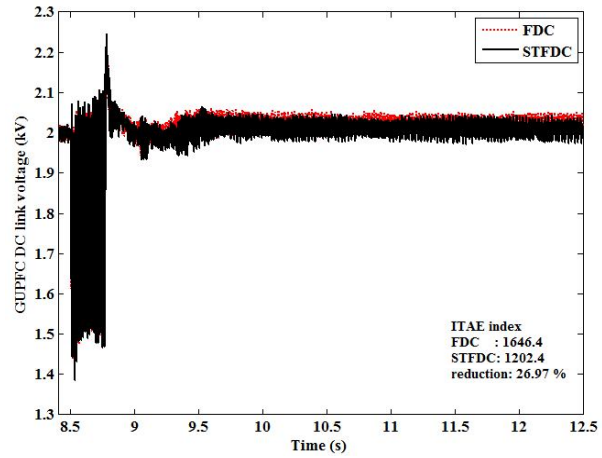

Fig. 12(g). DC voltage excursions of GUPFC under different control modes following single-phase fault

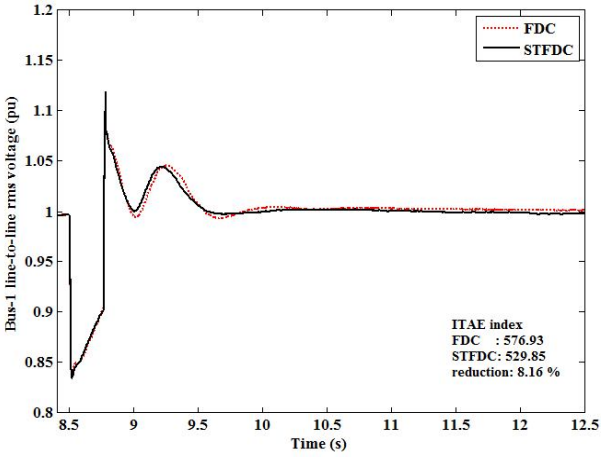

Fig. 12(h). Variation of Bus-1 voltage following single-phase fault

VII. Conclusion

The strong control capability of the GUPFC with regulating multi-line flows and bus voltage is extended with an optimized self-tuned fuzzy control scheme for oscillation damping in a wind farm integrated power system. It has been shown both graphically and quantitatively that the proposed damping scheme is robust in its performance over a range of disturbance conditions and does not only improves transient stability of induction/synchronous generators but also assists indirectly to other GUPFC control functions which are tightly interacted with each other. The proposed control scheme is model independent since the design is based on instantaneous system states rather than system parameters. With the inclusion of quasi-multi pulse converters switching at 60 Hz into the grid, harmonic content complies with the regulations. Hence, neither passive nor active filter is required for harmonic reduction or compensation at the ac side of the GUPFC converters. The study reveals the potential usage of GUPFC for intelligent control of future grids with distributed energy resources, along with low THD low loss power converters.

Since the simulated configuration relies on real-time communication of two programs, the increasing number of power system buses will adversely affect the simulation performance. Currently a dual-core modern CPU with 3 GBs of RAM dissipates around 1800 seconds for only one simulated second. To simulate more complex power systems embedded with STFDC based GUPFC, more CPU power with large memory requirements are highly demanded. Although the proposed damping controller is made generic as much as possible, the three gains of the STFDC should be re-optimized for a different power system configuration. This requires multiple-runs for optimization routine in the order of 50s.

References

[1] Z. Chen, F. Blaabjerg, Wind farm—A power source in future power systems, *Renewable and Sustainable Energy Reviews, vol. 13,issues 6–7*, August–September 2009, pp. 1288-1300.

[2] J.K. Kaldellis, D. Zafirakis, The wind energy (r)evolution: A short review of a long history, *Renewable Energy, vol. 36, issue 7*, July 2011, pp. 1887-1901.

Copyright © 2012 Praise Worthy Prize S.r.l. - All rights reserved

[3] H. Li, B. Zhao, C. Yang, H.W. Chen, Z. Chen, Analysis and estimation of transient stability for a grid-connected wind turbine with induction generator, *Renewable Energy, vol. 36, issue 5*, May 2011, pp. 1469-1476.
[4] A. Junyent-Ferré, O. Gomis-Bellmunt, A. Sumper, M. Sala, M. Mata, Modeling and control of the doubly fed induction generator wind turbine, *Simulation Modelling Practice and Theory, vol. 18, issue 9*, October 2010, pp. 1365-1381.
[5] R. Rabbani, A.F. Zobaa, Dynamic Performance of Wind Asynchronous Generators Using Different Types and Locations of Fault, *International Review on Modelling and Simulations (IREMOS), vol. 4, no. 6* (Part A), December 2011, pp. 2795-2801.
[6] C. Chompoo-inwai, W.J. Lee, P. Fuangfoo, M. Williams, J.R. Liao, System impact study for the interconnection of wind generation and utility system, *IEEE Transactions on Industry Applications, vol. 41, no. 1*, Jan.-February 2005, pp. 163- 168.
[7] N. Senthil Kumar, J. Gokulakrishnan, Impact of FACTS controllers on the stability of power systems connected with doubly fed induction generators, *International Journal of Electrical Power & Energy Systems, vol. 33, issue 5*, June 2011, pp. 1172-1184.
[8] P. Kundur,*Power system stability and control* (McGraw Hill, 1994).
[9] O. Samuelsson, S. Lindahl, On speed stability, *IEEE Transactions on Power Systems, vol. 20, n. 2*, May 2005, pp. 1179- 1180.
[10] X.P. Zhang, Modelling of the interline power flow controller and the generalised unified power flow controller in Newton power flow, *IEE Proceedings- Generation, Transmission and Distribution, vol. 150, no. 3*, May 2003, pp. 268- 274.
[11] X.P. Zhang, Restructured Electric Power Systems: Analysis of Electricity Markets with Equilibrium Models, *IEEE Press Series on Power Engineering*, 2010.
[12] A.M. Vural, K.C. Bayındır, Two-level Quasi Multi-Pulse Voltage Source Converter Based Generalized Unified Power Flow Controller, *International Review of Electrical Engineering (IREE), vol. 6, no. 5*, October 2011, pp. 2622-2637.
[13] R.K. Mudi, N.R. Pal, A robust self-tuning scheme for PI- and PD-type fuzzy controllers, *IEEE Transactions on Fuzzy Systems, vol. 7, no. 1*, February 1999, pp.2-16.
[14] S. Hameed, B. Das, V. Pant, A self-tuning fuzzy PI controller for TCSC to improve power system stability, *Electric Power Systems Research, vol. 78, issue 10*, October 2008, pp. 1726-1735.
[15] P.M. Anderson, A. Bose, Stability Simulation Of Wind Turbine Systems, *IEEE Transactions on Power Apparatus and Systems, vol. 102, no. 12*, December 1983, pp.3791-3795.
[16] C. Jauch, P. Sørensen, I. Norheim, C. Rasmussen, Simulation of the impact of wind power on the transient fault behavior of the Nordic power system, *Electric Power Systems Research, vol. 77, issue 2*, February 2007, pp. 135-144.
[17] P. Sørensen, A.D. Hansen, P.A.C. Rosas, Wind models for simulation of power fluctuations from wind farms, *Journal of Wind Engineering and Industrial Aerodynamics, vol. 90, issues 12-15*, December 2002, pp. 1381–1402.
[18] I. Erlich, J. Kretschmann, J. Fortmann, S. Mueller-Engelhardt, H. Wrede, Modeling of Wind Turbines Based on Doubly-Fed Induction Generators for Power System Stability Studies, *IEEE Transactions on Power Systems, vol. 22, no. 3*, August 2007, pp. 909-919.
[19] A. Kusiak, W. Li, Estimation of wind speed: A data-driven approach, *Journal of Wind Engineering and Industrial Aerodynamics, vol. 98, issues 10–11*, October–November 2010, pp. 559-567.
[20] E. Levi, General method of magnetising flux saturation modelling in d-q axis models of double-cage induction machines, *IEE Proceedings - Electric Power Applications, vol. 144, no .2*, March 1997, pp.101-109.
[21] H. Teng, C. Liu, M. Han, S. Ma, X. Guo, Synchronous Generator Model Transformation Between BPA And PSCAD, *Power and Energy Engineering Conference, APPEEC-2010 Asia-Pacific*, 28-31 March 2010, pp.1-4.
[22] IEEE Committee Rep, First benchmark model for computer simulation of sub-synchronous resonance, *IEEE Transactions on Power Apparatus and Systems, vol. 96, no. 5*, September-October 1997, pp. 1565–1572.
[23] S. Filizadeh, M. Heidari, A. Mehrizi-Sani, J. Jatskevich, J.A. Martinez, Techniques for Interfacing Electromagnetic Transient Simulation Programs With General Mathematical Tools, IEEE Taskforce on Interfacing Techniques for Simulation Tools, *IEEE Transactions on Power Delivery, vol. 23, no .4*, October 2008, pp. 2610-2622.
[24] J.A. Neider, R. Mead, A simplex method for function minimization, *The Computer Journal, vol. 7, no. 4*, 1965, pp. 308-313.
[25] A.M. Gole, S. Filizadeh, R.W. Menzies, P.L. Wilson, Optimization-enabled electromagnetic transient simulation, *IEEE Transactions on Power Delivery, vol.20, no. 1*, January 2005, pp. 512- 518.
[26] IEEE Recommended Practices and Requirements for Harmonic Control in Electrical Power Systems, Institute of Electrical and Electronics Engineering, April 1993.

Appendix

Controller parameters of GUPFC:

For shunt converter: K_{VQ}=8, T_{VQ}=0.02, K_{ED}=0.8, T_{ED}=0.01, for upper series converter: K_{D1}=1, T_{D1}=0.01, K_{Q1}=1, T_{Q1}=0.001, for lower series converter: K_{D2}=1, T_{D2}=0.01, K_{Q2}=1, T_{Q2}=0.001. K_w=500.

Wind turbine parameters:

2.5 MVA, w_B = 20 Hz, ρ = 1.225 kg/m^3, A= 5026 m^2 with a rotor radius of 40 m, gear box efficiency = 97 %, gear ratio (machine/turbine) = 55.

SEDCIG parameters:

2.5 MVA, 0.86 pf lagging (without fixed capacitors), V_{LL}=13.8 kV, base angular frequency=60 Hz, R_s = 0.066 pu, R_{r1}= 0.298 pu, R_{r2}=0.018 pu, L_s = 0.046 pu, L_m = 3.86 pu, L_{r1}=0.122 pu, L_{r2} = 0.105 pu, J=2H=3.40 s, mechanical damping = 0.01 pu.

SG parameters:

V_{LL}=13.8 kV, base angular frequency=60 Hz, pf= 0.9957, H = 3.117 s, mechanical windage and friction loss = 0.04 pu, iron loss = 300 pu, R_a = 0.0025 pu (armature time constant, T_a = 0.278 s), X_d = 1.014 pu, X'_d = 0.314 pu, T'_{d0} = 6.55 s, X''_d = 0.280 pu, T''_{d0} = 0.039 s, X_q = 0.770 pu, X''_q = 0.375 pu T''_{q0} = 0.071 s, potier reactance X_p = 0.163 pu, air gap factor = 1.0, number of Q-axis damper windings = 1.

IEEE type 2 Hydro Governor and turbine parameters:

for controller: real pole gain = 0.88, proportional gain = 3.7, integral gain = 0.44, real pole time constant = 0.02 s, Turbine lead time constant = 0.01 s, turbine lag time constant =0.01 s, governor time constant =0.05 s, inverse gate velocity limit =4.8 s/pu, gate velocity time constant =0.1 s, permanent droop gain =0.08, gate position control rate limit = 0.22 pu/s, temporary droop gain = 0.0, temporary droop time constant = 0.01 s, conversion constant = 0.895, time constant for smoothing = 0.02 s.

IEEE type SCRX solid state exciter parameters:

V_{LN} = 7967 V, line current=5020 A, rectifier smoothing time constant = 0.02 s**,** controller lead/lag time constant = 1.5/1.0 s**,** exciter time constant = 0.02 s**,** exciter gain = 100 pu**,** min/max field voltage = -+5 pu, reverse resistance = 15 kΩ.

Copyright © 2012 Praise Worthy Prize S.r.l. - All rights reserved

Authors' information

Ahmet Mete Vural was born in Turkey in 1976. He received his B.Sc. and M.Sc. degrees in electrical and electronics engineering (EEE) from University of Gaziantep, Gaziantep, Turkey in 1999 and 2001, respectively. From 1999 to 2004, he worked as a research assistant in EEE department in University of Gaziantep. From 2004 to 2007, he worked as a research assistant in Automation and Control Engineering Department in Wuppertal University, Germany. Now, he is working as instructor in EEE department in Gazikent University, Gaziantep, Turkey. He is currently working towards his PhD degree in EEE department in Cukurova University, Adana, Turkey. His research interests include modeling of multi-converter FACTS devices and their control.

Kamil Çağatay Bayındır was born in Turkey in 1973. He received his B.Sc. and M.Sc. degrees in electrical and electronics engineering (EEE) from Middle East Technical University ,Ankara, Turkey and PhD degree from Cukurova University, Adana, Turkey in 1995, 2000 and 2006, respectively. From 1997 to 2000, he worked as a research assistant in EEE department of Middle East Technical University. From 2000 to 2009, he worked as chief electrical engineer in petrochemicals industry,iron and steel industry. Now, he is working as Asst. Prof. in EEE department of Cukurova University, Adana, Turkey. His research interests include electrical power quality, custom power devices and FACTS devices, modeling of power electronics systems, energy management and efficiency.

Copyright © 2012 Praise Worthy Prize S.r.l. - All rights reserved

View publication stats